Mathematical Modeling of the Impact of Actin and Keratin Filaments on Keratinocyte Cell Spreading

Jin Seob Kim,[†*] Chang-Hun Lee,[†] Baogen Y. Su,[†] and Pierre A. Coulombe[†‡§*]
[†]Department of Biochemistry and Molecular Biology, Bloomberg School of Public Health, Johns Hopkins University, Baltimore, Maryland; [‡]Department of Biological Chemistry and [§]Department of Dermatology, School of Medicine, Johns Hopkins University, Baltimore, Maryland

ABSTRACT Keratin intermediate filaments (IFs) form cross-linked arrays to fulfill their structural support function in epithelial cells and tissues subjected to external stress. How the cross-linking of keratin IFs impacts the morphology and differentiation of keratinocytes in the epidermis and related surface epithelia remains an open question. Experimental measurements have established that keratinocyte spreading area is inversely correlated to the extent of keratin IF bundling in two-dimensional culture. In an effort to quantitatively explain this relationship, we developed a mathematical model in which isotropic cell spreading is considered as a first approximation. Relevant physical properties such as actin protrusion, adhesion events, and the corresponding response of lamellum formation at the cell periphery are included in this model. Through optimization with experimental data that relate time-dependent changes in keratinocyte surface area during spreading, our simulation results confirm the notion that the organization and mechanical properties of cross-linked keratin filaments affect cell spreading; in addition, our results provide details of the kinetics of this effect. These in silico findings provide further support for the notion that differentiation-related changes in the density and intracellular organization of keratin IFs affect tissue architecture in epidermis and related stratified epithelia.

INTRODUCTION

Keratinocytes are the major cellular constituents in the epidermis of skin, a surface tissue that provides an impermeable barrier and the first line of defense against potential damage from environmental exposures. Epidermal tissue integrity is essential to barrier function. It is maintained via epidermal differentiation as part of normal homeostasis and restored by wound healing after injury (1). Accordingly, the mechanical properties of keratinocytes play a crucial role in the skin's barrier function and properties as a tissue.

Intermediate filaments (IFs) are formed by the protein products of a large number of IF genes (>70) regulated in a tissue-, differentiation-, and context-dependent fashion (2,3). All major classes of IFs have been shown to provide structural and mechanical support that is vitally important to maintenance of cell and tissue integrity under stress. This role was initially revealed for keratin IFs in epidermis (4) and later extended to many additional types of tissue (2,5,6). Further, in vitro studies of purified reconstituted IFs showed that they must be cross-linked into a network to generate the elasticity and mechanical properties (7,8) necessary to sustain their mechanical support role in living cells (9,10). This basic principle also applies to actin filaments (11) and more generally to fibrous polymers (12).

Epithelial cells express type I and type II IF genes whose protein products copolymerize to form 10-nm-wide IFs in their cytoplasm. Specific combinations of type I and II keratin genes are expressed in a tissue-type-, differentiation-, and context-specific fashion in such cells (13). In addition to their biochemical composition, the intracellular concentration and organization of keratin IFs varies rather significantly depending on the cell type considered (2,4). In skin and related surface tissues, keratin IFs are unusually abundant ((14); also, J. S. Kim, C.-H. Lee, B. Y. Su, and P. A. Coulombe, unpublished data) and, in part because of their attachment at cell-matrix and cell-cell adhesion structures, exhibit a pancytoplasmic organization (15). On the one hand, such attributes underlie the ability of keratin IFs to perform a crucial role of mechanical support in the epidermis and related surface epithelia (16,17). Recent measurements confirmed that the keratin filament network makes a dominant contribution to the micromechanical (elastic) properties of human skin keratinocytes (18). On the other hand, these characteristics should enable keratin IFs to also act as key determinants of cell shape and tissue architecture in such settings.

We have been studying the property of self-organization of keratin filaments comprised of type II keratin 5 (K5) and type I keratin 14 (K14) pairing, which occurs in the progenitor basal layer of epidermis and related surface epithelia (16,19,20). As part of this effort, we recently uncovered the existence of an inverse relationship between the surface area of keratinocytes in two-dimensional culture ex vivo and the extent of keratin filament bundling in their cytoplasm (20). This latter evidence implies that the organization and mechanical properties of keratin IFs affect

Submitted March 29, 2012, and accepted for publication September 4, 2012.

*Correspondence: jskim@jhsph.edu or coulombe@jhsph.edu

Jin Seob Kim's present address is Institute for NanoBio Technology, Johns Hopkins University, Baltimore, MD 21218.

Chang-Hun Lee's present address is College of Basic Science, School of Convergence, Daegu Gyeongbuk Institute of Science & Technology, Daegu, 711-873, Korea.

Editor: Charles Wolgemuth.

0006-3495/12/11/1828/11 $2.00

http://dx.doi.org/10.1016/j.bpj.2012.09.016

keratinocyte morphology and epidermal architecture. Here we report on a successful effort to devise a simple theoretical model to investigate and substantiate this relationship.

MODEL

Background information

The mechanism of cell spreading is inherently complex, as suggested in recent studies on the spreading of mouse embryonic fibroblasts (21,22). At a very early stage after their attachment to the substratum, the spreading of cells in a two-dimensional culture setting follows a universal law (23). The timescale of this initial stage is very short (<15 min), although its magnitude varies depending on various elements, including cell type. Experimental evidence shows that the microtubule-organizing center generally does not have a significant impact on cell spreading (23). Protrusion events originating from cycles of actin polymerization and depolymerization and branching in the cortical area of the cell are considered a key factor at this stage (24). Experimental studies of cell spreading further show that cell contact area initially increases monotonically at a rate that depends on the concentration of relevant ligands in the substratum (21,22,24–28).

After this early stage, cells eventually become flattened and display a well-developed cytoskeleton, including an elaborate actomyosin system and a well-spread network of IFs. These elements are predominant in the lamellum, i.e., the subcellular area that extends from the edge of the nucleus to the lamellipodium at the distal edge of the cell (Fig. 1 *B*). At this stage, the cell exhibits two distinct actin filament networks: a relatively narrow one featuring a branched architecture and undergoing classical treadmilling that drives spreading in the distally located lamellipodium zone, and another, broader one organized as stress fibers and co-existing with IFs in the lamellum zone extending from the lamellipodium to the nucleus (Fig. 1 *B*) (25,29).

After the initial stage, the mechanisms underlying spreading are believed to be the same as those driving cell motility (22). Actin treadmilling at the leading edge drives lamellipodial protrusion and, as a result, lamellum expansion (29,30). The retrograde flow velocity of actin is also known to be important for lamellipodial protrusion (31). Another key regulator of spreading and motility is adhesion to the extracellular matrix (32). Small and nascent focal adhesions (FAs) near the leading boundary of the spreading or moving cell generate strong propulsive forces, whereas larger and mature adhesion sites located inside the cell, behind the leading edge, exert weaker forces (33). Assembly and stabilization of nascent FAs in the lamellipodium occurs in an actin-dependent but myosin-II-independent fashion, whereas their subsequent maturation is regulated by opposing influences from α-actinin-mediated actin cross-linking and myosin II activity (34). The lamellipodium thus behaves like a caterpillar, given polymerization-driven forward movement at the leading edge and net disassembly at the rear boundary. At this latter end, a subset of FAs disassembles, whereas others undergo maturation with the help of α-actinin and myosin II. Myosin II activity is known to be inversely proportional to cell spreading, possibly due to the increasing mechanical or viscoelastic properties of the cytoplasmic network (26).

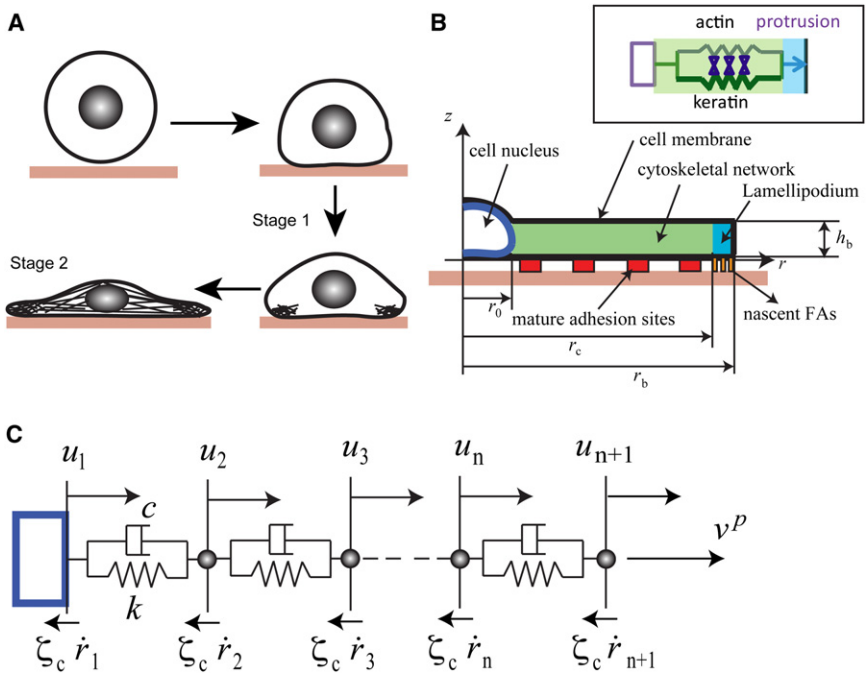

FIGURE 1 Graphical explanation of the model. (*A*) Cartoon depicting our two-stage model assumption. (*B*) Continuum mechanical model for stage 2. (*Inset*) Graphical representation of the interconnection between F-actin and keratin IF networks. (*C*) Finite-element version of the continuum mechanical model for stage 2. Each element is represented by an elastic spring (k) and a dashpot (c), which emphasizes that the model uses the viscoelastic continuum model. Here, u_i denotes the nodal displacement. Friction forces from mature adhesion sites are denoted as $\zeta_c \dot{r}_i$.

Description of the model

Given our measurements on keratinocytes in two-dimensional culture (Figs. 2 and 3 *A*), in this study, we divide the spreading of nondividing cells into two discrete stages, 1 and 2 (Fig. 1 *A*). Stage 1, the initial stage, occurs at a constant protrusion speed, v_0^p. We have

$$r(t) \sim v_0^p\, t, \tag{1}$$

conveying that lamellipodial protrusion is the most influential determinant of cell spreading during stage 1.

Our modeling effort primarily focuses on stage 2 (Fig. 1 *A*), when the spreading cell has flattened, the actin and keratin networks are cross-linked and established, and the shape and mechanical properties of the nucleus are set (see below). As a first approximation for modeling stage 2, we assume a cylindrically symmetric shape for the cell (with a circular plate shape in top view), resulting in isotropic cell spreading. Mathematically, we can afford to consider only the cross-sectional area of the cell. Our model ignores deformation of the nucleus, in part because it has been shown to be much stiffer than the cytoplasm (35,36). Further, from stage 2 onward, spreading continues to be driven primarily by events occurring in the lamellipodium (distal edge) and their dynamic interplay with the cytoskeleton and adhesion events in the lamellum (main cytoplasmic space). We note that experimental measurements show that the nucleus does not deform much during this second stage of cell spreading (see below).

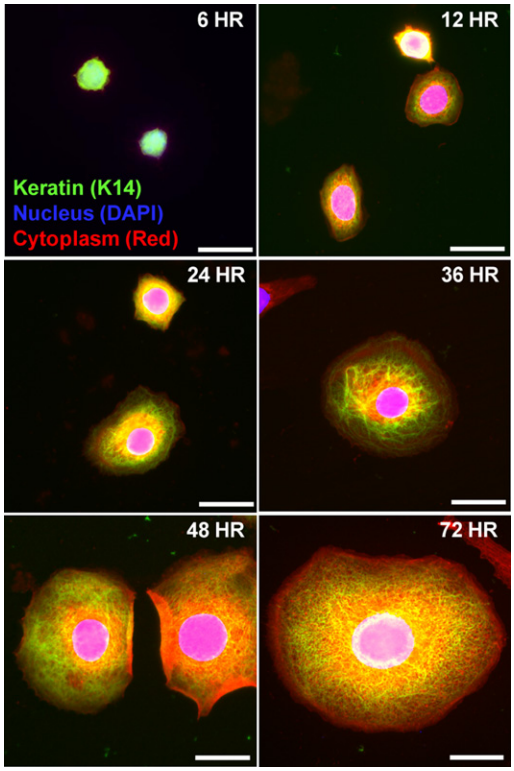

FIGURE 2 Micrographs of spreading mouse skin keratinocytes at different time points during cell spreading (scale bar, 20 μm). We systematically eliminated outlier data by retaining all measurements falling within the 95% confidence interval for each time point. This time course reveals the development and maturation of the cytoskeletal network with time. After $t = 36$ h, the cytoskeletal network appears to be fully developed.

The resulting simplified model is conveyed in Fig. 1 *B*. Given that variations in height should be smaller compared to other geometrical dimensions during stage 2 (also see the Supporting Material from Krzyszczyk and Wolgemuth (31)), here we treat this quantity as constant, $h_b = 200$ nm. This value corresponds to the thickness of the lamellipodium (30,37). With this, the phenomenon being modeled can be formulated using a one-dimensional partial differential equation. The geometry of the relevant portion of the cell can be described using cylindrical coordinate systems in the continuum mechanics formulation. r denotes the coordinates inside the cell body, and r_0 and r_b denote the coordinates of the nucleus and boundary, respectively (Fig. 1 *B*). r_0 is assumed to be constant in our model.

We further assume that the network is uniformly and symmetrically distributed. We treat the actin and keratin networks (cross-linked or not) as a continuum of viscoelastic material. Important factors to consider include the mechanical properties of cross-linked F-actin and keratin IF networks, forces emanating from adhesion sites, and protrusion events along the edge of the cell outer membrane. The elastic property of each cytoskeletal network is described by two different sets of mechanical properties, Y_f and ν, respectively denoting the Young's modulus and Poisson's ratio. The viscosity of each network is described by the relaxation modulus, μ_1. As outlined in the Supporting Material, we rely on published data describing the mechanical attributes of keratin filament assemblies (8) and skin keratinocytes (18).

Generally speaking, cytoskeletal networks may undergo large deformations as a cell spreads. In that case, finite deformation continuum modeling might be more appropriate. Therefore, we use the compressible finite linear viscoelastic constitutive relation in this study. A detailed explanation is given in Kim and Sun (38). In general, the viscous part of the stress is linear with respect to strain velocity and may include memory effects. For motion over a relatively long timescale, which applies here, such memory effects may be neglected. The time constant specific to the viscoelastic properties of the cytoskeleton is ~1 s (9,39). Hence, we use the constitutive relationship (38)

$$\begin{aligned}\boldsymbol{\sigma}(\mathbf{x},t) \;=\; & (\lambda_0 \ln\det \mathbf{A} - \mu_0)\,\mathbf{1} + \mu_0 \mathbf{A}\mathbf{A}^T \\ & + \frac{\mu_1}{2}\left(\dot{\mathbf{A}}\mathbf{F}^{-1} + \mathbf{F}^{-T}\dot{\mathbf{A}}^T\right),\end{aligned} \tag{2}$$

where $\mathbf{F}$ and $\mathbf{A}$ denote the so-called deformation gradient tensors for total and elastic deformation, respectively.

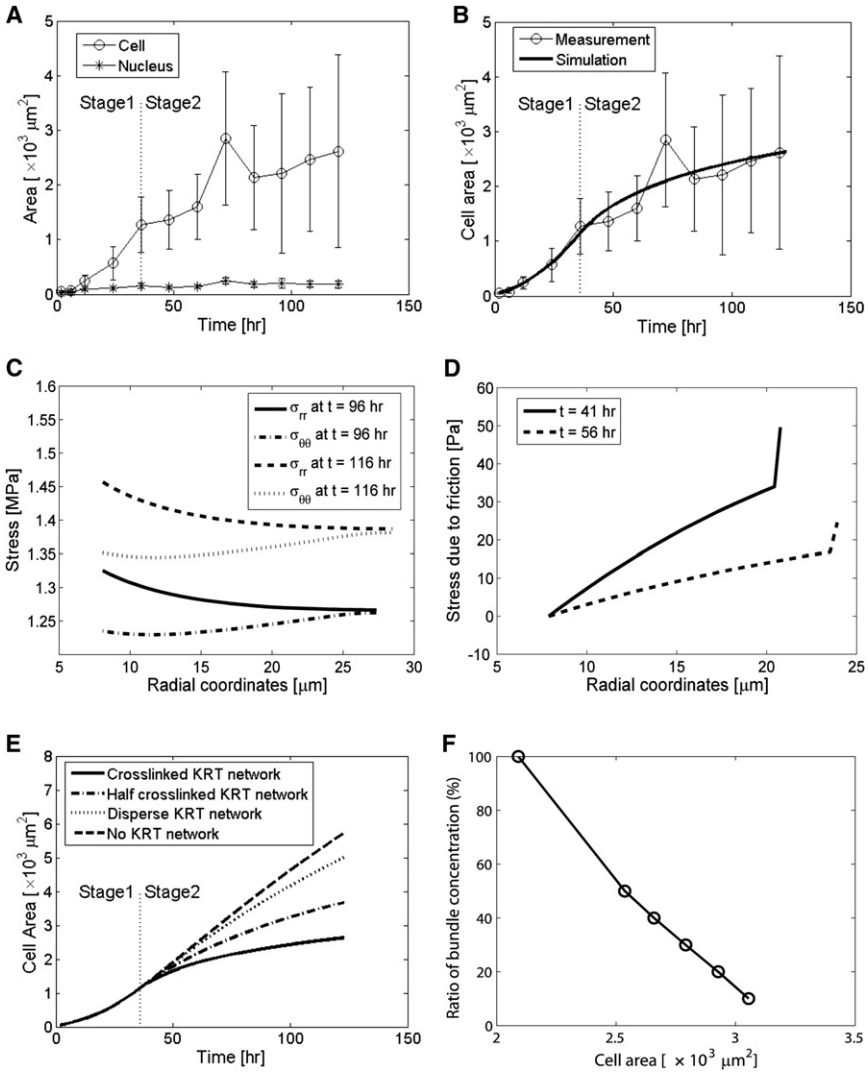

FIGURE 3 Measurement data and simulation results for wild-type mouse skin keratinocytes. (*A*) Measurements of spreading area of cells and nuclei. Error bars represent the standard deviation. (*B*) Simulation results with optimized parameters: $v_0^p = 0.0072$ μm/min and $\gamma = 1.85 \times 10^{-10}$ μm. (*C*) Stress distribution developed in the cytoskeletal network. (*D*) Frictional stress due to mature adhesion sites. (*E*) Cell spreading area with varying degrees of filament bundling in the keratin IF network. (*F*) Our simulation shows an inverse correlation between the degree of filament bundling in the keratin IF network and cell surface area, which confirms and extends the result reported by Lee and Coulombe (20).

Here, we denote Lamé constants as λ_0 and μ_0, which are directly related to Young's modulus and Poisson's ratio. μ_1 is the relaxation component of the viscoelastic moduli.

Actin polymerizes at the leading edge of the lamellipodium, causing protrusion, and depolymerizes at its rear boundary. Distal events are treated simply via a protrusion speed, v^p, and it is assumed that the lamellipodial width (Fig. 1 *B*) stays constant during cell spreading. In other words, the lamellipodium behaves like a particle. It ensues that protrusion speed corresponds to the speed of a particle located at $r = r_b$, implying that we set $r_b = r_c$ in Fig. 1 *B*. Further inside the cell, the lamellar cytoskeleton (Fig. 1 *B*, *green domain*) undergoes growth and maturation during cell spreading. In this case, we utilize the concept of growth as described in Kim and Sun (38), with the deformation gradient tensor $\mathbf{G}$.

The actin and keratin networks are treated as separate but interdependent entities in our model. When appropriate, quantities of interest are dressed with a tilde to denote keratin networks. For example, Y_f and $\tilde{Y}_f$ denote the Young's moduli of actin and keratin networks, respectively. We posit that the keratin network is attached at or near mature adhesion sites near the rear boundary of the lamellipodium (40). In Kölsch et al. (41), keratin IFs were seen to behave like a ruptured spider network upon disruption of actin, pointing to the existence of interconnections between them (see Fig. 1 *B*, *inset*, and Green et al. (42)). We infer that the cross-linking between the actin and keratin networks is of a rigid nature compared to their other elastic features. Mathematically, therefore, the F-actin and keratin IF networks share the same displacement fields in the lamellar cytoplasm. In other words,

$$u\,(r) \;=\; \tilde{u}\,(r). \tag{3}$$

In this case, total stress in the cytoskeletal network is computed as

$$\boldsymbol{\sigma}^t \;=\; \boldsymbol{\sigma} + \tilde{\boldsymbol{\sigma}}. \tag{4}$$

Therefore, the equation of motion is

$$\frac{\partial \sigma_{rr}^{t}}{\partial r} + \frac{1}{r}\left(\sigma_{rr}^{t} - \sigma_{\theta\theta}^{t}\right) = \varsigma_c v_r. \quad (5)$$

The actual form of this equation depends on the treatment of cytoskeletal networks. The most general consideration is that both the F-actin and keratin IF networks undergo growth (applied from this point forward). We employ the finite-element method to solve the equation of motion (see schematic in Fig. 1 *C*). Detailed formalism with boundary conditions can be found in the Supporting Material.

Lamellipodial protrusion and growth in the cytoskeletal network

In our model, the F-actin and keratin IF networks adhere to the same growth law based on the aforementioned information. As the lamellipodium rolls outward at the leading edge, some of the nascent FAs are destined to form mature adhesion sites. Given a weak coupling of the lamellipodium and lamellum in the materialistic sense (29), we assume that stress in the cytoskeleton represents a key influence on lamellipodial protrusion speed. To be more specific, cytoskeletal stress in the lamellum is assumed to trigger biochemical signaling pathways that impact the rate of polymerization/depolymerization of actin filaments in the lamellipodium. The latter is consistent with the notion that mechanical stress can be transduced into biochemical signals through cytoskeletal deformation (43). With this information, we propose that protrusion speed in the lamellipodium is a function of forces acting at its boundary with the lamellum. Mathematically it can be written at the *k*th time step as (38)

$$v^{p} = v_0^{p}\, e^{-\gamma\, \sigma_{rr}^{t}(r_b, t_{k-1})\, 2\pi\, r_b h_b / k_B T}. \quad (6)$$

This mimics the force-protrusion velocity of the lamellipodium as reported in Mogilner and Oster (44). v_0^p, the constant protrusion speed of the lamellipodium (cf. above), is known from considering stage 1. γ is a constant that represents, in units of μm, the characteristic dimension related to the work achieved by force. $\sigma_{rr}^{t}(r_b, t_{k-1})\, 2\pi\, r_b h_b$ represents the force acting on the surface at $r = r_b$.

Next, let us discuss the growth law applying to the cytoskeleton. The lamellipodium and lamellum feature distinct F-actin networks that are continuously linked, albeit weakly in the materialistic sense, and that differ in kinematics (G-actin inward flow), kinetics (turnover or net assembly of F-actin), and material properties (29). Yet we assume that both lamellipodial protrusion and lamellum expansion are mainly governed by net F-actin assembly. We propose the following model for the growth of the cytoskeletal network:

$$u_g(r, t_i) = \alpha\, u(r, t_i - \tau)\, \delta(r - r_b), \quad (7)$$

where u_g denotes displacement due to the cytoskeletal growth, which defines **G** (cf. previous section). Here, τ denotes the time lag between lamellum formation and lamellipodial protrusion, and α is a proportional coefficient. The origin of α can first be inferred from the fact that kinetics in the lamellipodium and lamellum are different, as conveyed in Ponti et al. (29). Two spatial maxima of net F-actin assembly rate are considered. One maximum occurs in the lamellipodium per se and is related to the protrusion speed, whereas the other coincides with the outer boundary of the lamellum. α reflects the difference in magnitude between these maxima, and is assumed to be 0.3 (29). The specific location of the second local maximum is conveyed by the term $\delta(r - r_b)$ in the above equation. Our model assumes, it is important to note, that growth of the lamellum in response to lamellipodial protrusions occurs near its distal boundary. Further, the sinusoidal pattern exhibited by the net assembly rate of F-actin in the lamellipodial area in Ponti et al. (29) verifies our assumption that it moves like a rolling caterpillar. The mathematical rationale for Eq. 7 can be found in the Supporting Material.

Actomyosin activity can pull actin filaments and affect cell spreading by contributing to the development of higher stress. Such myosin-related stress was assumed to be $10^2 - 10^3$ Pa in a previous modeling effort (45). This actomyosin effect could be included in our modeling effort. However, since we lack detailed information about both the temporal and spatial distribution of this active stress in the epidermal keratinocytes being studied, and given that the magnitude of this active stress is likely smaller than other elastic properties of the network, we opted here to ignore this active effect. Also, our experimental results (see Fig. S1 and Fig. S2) show that stress related to myosin activity does not seem to significantly affect the spreading of keratinocytes.

The cell radius does not increase in a continuous, monotonic fashion during spreading (25). Instead, it shows a transient and stochastic behavior, denoted as stochastic transient extension periods (STEPs). The duration of these periods was estimated to be 25 s or so for a half-cycle, either in the anisotropic or late isotropic cell-spreading mode. This phenomenon is likely related to the balance resulting from actin polymerization and retraction (25). Retraction is thought to stem from the activity of myosin and α-actinin and is related to the formation of mature focal adhesions in the lamellum (29,46). Consequently, one might expect that the boundary between the lamellipodium and the lamellum moves with a time lag relative to the lamellipodial protrusion (see Ponti et al. (29)). In our model, we incorporate full-cycle STEPs as the time lag, i.e., $\tau = 1$ min, to reflect the effect of retraction and recovery of the movement of the lamellum-lamellipodium boundary on the lamellum formation in response to the lamellipodial protrusion.

The material parameters used in our simulations are listed in Table 1 (see the Supporting Material for a detailed

TABLE 1 Parameters of the cytoskeletal network for the continuum mechanical model

Description	Value
Young's modulus for F-actin network, Y_f (kPa)	20
Young's modulus for cross-linked keratin IF network, $\tilde{Y}_f$ (kPa)	117
Young's modulus for disperse keratin IF network, $\tilde{Y}_f$ (kPa)	8.66
Poisson's ratio	0.49
Viscous modulus, μ_1 and $\tilde{\mu}_1$ (Pa·min)	1.67
Friction coefficient due to mature adhesion, ς_c (pN·min/μm^4)	5×10^4

explanation of how these parameters were obtained, and how we estimated the Young's modulus for partially cross-linked keratin networks).

EXPERIMENTAL METHODS

Newborn mouse skin keratinocytes were isolated and grown at 37°C in primary culture on collagen-IV-coated coverslips as described previously (20,47). At select intervals after the initial attachment, cells were fixed with buffered 3.3% paraformaldehyde and processed for indirect immunofluorescence. The keratin network was imaged using a rabbit polyclonal anti-K14 antibody (Covance, Princeton, NJ) followed by Alexa Fluor 488-conjugated goat antirabbit IgG (Invitrogen, Carlsbad, CA). The cytoplasmic space was visualized using Alexa Fluor 594-C5-maleimide (Invitrogen) after treatment with Bond-Breaker-TCEP (Thermo Scientific, Waltham, MA) which makes cysteine residues in the cytoplasmic proteins stay available for fluorescence labeling, and the nucleus was stained with DAPI dye (Invitrogen).

For the myosin II inhibition studies, keratinocytes were grown and processed exactly as described above, except that they were exposed to 10 μM blebbistatin (or the same volume of dimethylsulfoxide vehicle as control) at every 12-h time point. For each treatment, a 10 mM stock solution of blebbistatin was diluted freshly at a 1:1000 ratio with mKER medium immediately before addition to cell cultures.

Human dermal fibroblast HDFn were purchased from Life Technologies (Grand Island, NY) and grown in M106 medium supplemented with 5% fetal bovine serum. Cells were seeded on collagen-coated coverslips and placed in a 37°C incubator for 30 min before incubation with or without 10 μM blebbistatin for an additional 30 min. At the end of the treatment time period, cells were fixed and stained with Alexa Fluor 594-C5-maleimide, and the cytoplasmic area was analyzed according to the procedure described for keratinocytes.

Cells were imaged using a fluorescent microscope (Axio Observer Z1 microscope with AxioCam MRm; Carl Zeiss, Oberkochen, Germany) fitted with a 40×, 1.3 NA EC Plan-NeoFluar Oil DIC M27 objective lens. Microscope operation and image acquisition were done using the AxioCam software (Carl Zeiss). To measure the surface area of entire cells and nuclei, recorded micrographs were processed using ImageJ software to yield 8-bit binary images. Relevant areas were computed by counting the number of pixels in the processed images using the Analyze Particles command.

RESULTS

Cell-spreading measurements

We measured the surface area of the entire cell and of its nucleus, as wild-type newborn (P2) mouse keratinocytes undergo spreading after they are seeded for primary culture (Figs. 2 and 3 *A*). We systematically eliminated outlier data by retaining all measurements falling within the 95% confidence interval for each time point considered. We calculated the radius of the nucleus at equilibrium to be $r_0 = 7.9$ μm by interpolation using an $a\,(1 - e^{-b\,t})$ type of function.

Our purpose and strategy require that we establish the timing of the transition between stages 1 and 2 as they apply to newborn mouse skin keratinocytes. This information can be inferred from the observed spreading kinetics of these cells in ex vivo culture (Figs. 2 and 3 *A*). An inflection point occurs at $t = 36$ h (Fig. 3 *A*) and is here taken to reflect this transition. Further, morphological analyses show that cytoskeletal networks are not yet fully developed at $t = 24$ h, but have reached a stable configuration by $t = 36$ h (Fig. 2), lending support to the inference made from the quantitative measurements (Fig. 3 *A*). Beyond $t = 36$ h, therefore, the mechanism of cell spreading can be assumed to be largely the same as that prevailing during cell migration (see Introduction).

Simulation results with wild-type keratinocytes

As mentioned in the previous section, the model for stage 1 is written as

$$r_b = v_0^p(t-6) + A_{\text{meas}}[t = 6], \tag{8}$$

in units of hours for time t. Equation 10 and the continuum model for stage 2 outlined above were combined and integrated with the experimental measurements of cell area reported in Fig. 3 *A*.

Optimization was performed using the fminsearch function in Matlab (The MathWorks, Natick, MA), giving rise to $v_0^p = 0.0072$ μm/min and $\gamma = 1.85 \times 10^{-10}$ μm, along with the simulation reported in Fig. 3 *B*. These parameters are considered intrinsic to wild-type skin keratinocytes.

Next, stress developed in the cytoskeletal network, as well as friction stress due to mature adhesion sites, were incorporated, as shown in Fig. 3, *C* and *D*, respectively. In Fig. 3 *C*, σ_{rr} and $\sigma_{\theta\theta}$ refer to the radial and circumferential components of cytoskeletal stress. These two types of stress increase with time, as expected. The existence of residual stress in the cytoskeletal network can be inferred from the experimental observation that a cell retracts when its adhesion to the substrate is reduced (25).

There have been experimental studies on the traction forces exerted on the substrate by migrating or spreading cells (27,48). When cells spread, mechanical stresses or forces are transferred onto the substrate through adhesion-related friction. In our model, friction stress due to adhesion is the quantity corresponding to the measured traction stress. As expected from the time-dependent decrease in cell spreading rate, stress due to friction decreases with time, since friction is proportional to the velocity of the cytoskeletal network. The resulting distribution of friction-related stress (Fig. 3 *D*) agrees well with traction measurement results obtained on fibroblasts (i.e., larger near the boundary and smaller inside the cell) (27,48). However, the actual

magnitude of the friction stress might differ for skin keratinocytes and is affected by substrate stiffness, ligand density, and adhesion molecules at the cell surface. We also note that our assumption of constant friction coefficient may not be accurate: in reality, the friction coefficient originating from mature adhesion-site formation is not necessarily constant. Note that μ_1 does not affect cell spreading, essentially because we do not consider memory effects (see Eq. 2).

Prediction on the impact of keratin network on cell spreading area

Next, simulations of keratinocyte spreading were conducted in the absence and presence of a keratin filament network, and with different degrees of cross-linking. The Young's modulus originating from keratin filaments was adjusted to convey these various circumstances. In Fig. 3 *E*, cross-linked and dispersed keratin networks represent circumstances in which wild-type keratin filaments are fully bundled and unbundled (disperse), respectively. On the other hand, half cross-linked represents the case where the extent of keratin IF bundling is lessened owing to any number of physiological circumstances (20). At a practical level, we simply varied the concentration of keratin, as discussed in the Supporting Material, to examine the impact of varying degrees of keratin IF bundling. The outcome of our simulation points to an inverse correlation between the occurrence of keratin filament bundling (Fig. 3 *F* and Movie S1), the degree to which is occurs, and the temporal evolution of the keratinocyte surface area (Fig. 3, *A* and *B*). These simulation results closely match the experimental data previously reported (compare Fig. 3 *B* with Fig. 4 *o* in Lee and Coulombe (20)). Various elements make it inappropriate to directly compare and relate the simulation and experimental data sets.

Altogether, the outcome of these simulations confirms and extends the notion that keratin IFs represent a mechanically important element in the cytoskeleton that is poised to impact cell morphology during cell spreading. This is likely to apply as well to keratinocyte migration, and to terminal differentiation in epidermis and related epithelia in situ.

Effect of friction on cell spreading

Adhesion events are among the key factors known to affect cell spreading and migration. In our model, the effect of adhesion events is incorporated as friction, as has been done in previous modeling efforts focused on cell migration (45,49). We next varied the friction coefficient in our model to gauge the impact of adhesion-related forces on cell spreading (Fig. 4). Two cases were compared, $\varsigma_c = 5 \times 10^6$ pN·min/μm^4 (Fig. 4, *A*, *C*, and *E*) and $\varsigma_c = 2.5 \times 10^8$ pN·min/μm^4 (Fig. 4, *B*, *D*, and *F*). There has been no explicit effort to assess the relation between the friction coefficient and the corresponding stress, and we selected these values so as to vary frictional stress by a 50-fold factor (see Fig. 4, *E* and *F*). First, let us look at the former case. The corresponding spreading area remains very similar to that reported in Fig. 3 *B* (with $\varsigma_c = 5 \times 10^4$ pN·min/μm^4). However, a small change occurs in stress distribution within the cytoskeletal network (Fig. 4 *C*), as follows: stress in the region close to the nucleus decreases, whereas stress in the boundary region increases compared to Fig. 3 *C*. The spatial distribution of stress due to friction does not change appreciably, except for its order of magnitude, which now seems closer to previously reported measurements (27,49). This result suggests that, once mature, adhesion sites do not make a significant contribution to cell spreading. Instead, factors related to protrusion should be crucial, as is likely the case in general cell dynamics. When the friction coefficient is increased to $\varsigma_c = 2.5 \times 10^8$ pN·min/μm^4, however, there is a marked difference in spreading area (Fig. 4 *B*). Further, the stress developed in the cytoskeletal network is significantly altered (Fig. 4 *D*). Relative to the situations modeled to this point, there is a higher stress distribution at boundary regions, generating a negative impact on protrusion speed (cf. Eq. 6) and cell surface area at equilibrium. Under this circumstance, higher friction near the boundary is developed at an earlier time point (Fig. 4 *F*, $t = 41$ *h vs.* $t = 56$ *h*) in cells undergoing spreading, unlike the previous cases, where friction development increases monotonically from the perinuclear region. The outcome of these simulations implies that cells do not spread or move much when exhibiting very large and stable mature adhesion sites (as conveyed by experimental findings involving FAK-null fibroblasts (50)), and help establish the validity of our modeling and its assumptions.

DISCUSSION AND CONCLUSION

In surface epithelia, keratin filaments occur at a very high density and form a cross-linked or bundled cytoplasmic network that provides mechanical resilience against external stresses. An open issue of significant interest is whether, and how, the cross-linking or bundling of keratin IFs affects cell morphology. Following up on the observation that the degree of keratin IF bundling negatively impacts keratinocyte cell spreading area in the two-dimensional cell culture setting (20), we developed a mathematical model in which actin and keratin networks in the cytoplasm are treated as a continuum to assess the impact of keratin filament cross-linking on keratinocyte cell spreading.

The mathematical model divides the cell spreading process into two stages. In stage 1, our model recognizes that protrusion events in the lamellipodium dominate the initial phase of cell spreading. In stage 2, corresponding to the primary focus of our study, the interplay between lamellipodial protrusion at the distal edge, the cytoskeletal

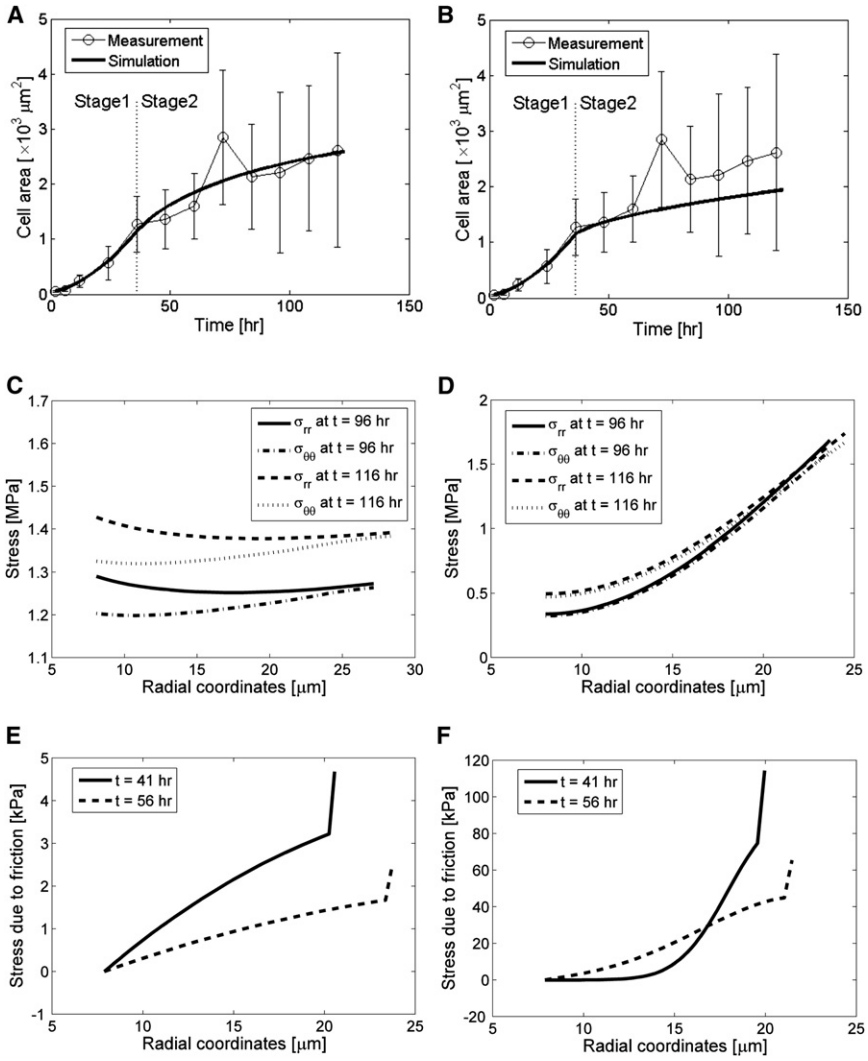

FIGURE 4 Effect of friction coefficient on cell spreading. Cell surface area (*A* and *B*), components of cytoskeletal stress (*C* and *D*), and frictional stress due to mature adhesion sites (*E* and *F*) from two different cases: $\varsigma_c = 5 \times 10^6$ pN·min/μm^4 (*A*, *C*, and *E*) and $\varsigma_c = 2.5 \times 10^8$ pN·min/μm^4 (*B*, *D*, and *F*). A higher friction coefficient (increase by 50-fold) yields smaller cell surface area and markedly altered stress and frictional stress distributions.

network that has formed in the lamellum (i.e., the main cytoplasmic space), and adhesion events is described in a continuum mechanical fashion. We proposed simple mathematical laws for lamellipodial protrusion and cytoskeletal growth at this second stage. The law for lamellipodial protrusion mimics the well-known Bell's equation (51), where actin assembly rate in the lamellipodium is influenced by a force signal originating from the cytoskeletal network in the lamellum. The growth law for the lamellar cytoskeleton incorporates phenomenological descriptions of cell spreading and migration. Two key parameters in our model were inferred from the observed spreading kinetics of newly attached keratinocytes in primary culture. The outcome of our modeling efforts confirms that cross-linking of keratin IFs affects cell surface area. The impact of this cross-linking can be abstracted through the concept of active force transmission within the cytoskeletal network. We propose that as they undergo bundling and/or cross-linking, keratin filaments develop additional tensile stress in the cytoskeleton, which in turn affects protrusion of the lamellipodia. It is important to note that the model we developed verifies the inverse correlation between cell contact area and the extent of bundling and/or cross-linking of keratin IFs in the cytoskeleton (20). Moreover, our model predicts that cell-protrusion formation should be stimulated in a direction opposite that of the keratin network, and should thereby promote polarized cell migration, as observed in Weber et al. (52).

The determinants of spreading, and the impact of the IF network, likely differ depending on the specific circumstances of the cell and, just as important, cell type. The spreading of fibroblasts in culture has been studied (21,22,26) and modeled (45) by others, and there are several differences between those studies and our effort. Vimentin is the main IF protein expressed in fibroblasts, where it plays several important roles, including having an impact on cell shape and cell motility during the epithelial-to-mesenchymal transition (53). Of note, the vimentin IF network is localized mostly in the nonmoving part of the cytoplasm in motile fibroblasts (54). Further, fibroblasts increase their

spread area rather rapidly upon myosin inhibition (26), a finding that we have confirmed, whereas keratinocytes respond much more slowly, and in fact contract, in response to the same treatment (Fig. S1). Blebbistatin-treated keratinocytes show increased keratin bundling, consistent with our experimental (20) and modeling (this study) findings that the extent of keratin IF bundling impacts cell spreading area. These observations call for circumspection in relating our findings to other types of cells, and other types of IF systems.

The model we introduce here also highlights the cooperation between the keratin IF and F-actin networks to regulate cell spreading and, by extension, cell surface area. An assumption made to attain this finding is the occurrence of rigid linkages between keratin IFs and F-actin, a well-established determinant of cell morphology (55). There is experimental evidence that keratin IFs interact and undergo cross talk with the F-actin network (41,42,56), though the physical attributes of the interconnection remain poorly understood. Loss of select keratins, e.g., K6, significantly affect F-actin organization in mouse skin keratinocyte cultures (57). Also, our data highlight the possibility of cross talk between actomyosin and keratin IF networks (see Fig. S2). A possible linking mechanism between the keratin and F-actin networks involves plectin (58,59). Plectin occurs in multiple isoforms, has side arms that can bind MTs, F-actin, and IFs (60), and has already been shown to significantly affect cytoskeletal organization (61). In two-dimensional culture, plectin-null newborn mouse skin keratinocytes exhibit increased F-actin stress fibers along with increased keratin IF bundling (62). Of further interest, loss of either K6 (63), plectin (62), or plakoglobin, an IF-interacting adhesion plaque molecule (64), result in increased Src activity in mouse skin keratinocytes, conveying that cytoskeletal elements are also integrated via powerful signaling pathways. A distinct, and complementary, mechanism to mediate such cytoskeletal interconnections would be the occurrence of direct physical contact between them. Specifically, keratin IFs could be trapped in the branches of the F-actin network (42).

Keratinocyte size in two-dimensional culture strongly correlates with their clonogenic and proliferation potential, and with differentiation (65–68), all of which are fundamental attributes of epidermis and related epithelia in vivo. A broader issue, therefore, is whether keratin IF organization is a driver or a consequence of the striking changes that occur in cell shape, size, and orientation as keratinocytes undergo terminal differentiation in epidermis and other stratified epithelia. Keratinocytes are columnar and oriented perpendicular to the epidermal axis in the basal layer, become roughly polygonal in the early spinous (early differentiating) layer, and then flatten and reorient parallel to the epidermal axis in the late spinous and granular (late differentiating) layers. The latter process features a progressive increase in the concentration of keratin filaments (14), and in the degree of their bundling, along with striking changes in the density and distribution of desmosome cell-cell contacts, to which they attach. One can readily conceive, therefore, that increases in filament density and bundling can, in a desmosome (and maybe in F-actin) attachment-dependent fashion, promote cell flattening during differentiation. The model we introduce here provides a framework upon which to investigate this intriguing possibility and its consequences for epidermis homeostasis. In the course of devising this model, we became aware of the paucity of quantitative data about several fundamental attributes of a tissue like the epidermis. To single out one example, there is very little known about the density and distribution of cell-cell adhesions, whether actin-linked or keratin-linked, in the three-dimensional context of epidermis. The advent of sophisticated microscopy techniques to map, with sufficient resolution, the localization of molecules in the three-dimensional framework of tissues represents a key advance that will make it possible to secure the missing information to better understand the genesis and maintenance of tissue architecture, as well as its functional ramifications.

SUPPORTING MATERIAL

Supporting Methods, three figures, one movie, and additional references are available at http://www.biophysj.org/biophysj/supplemental/S0006-3495(12)01030-2.

The authors are grateful to members of the laboratory for support.

This work was supported in part by grant AR42047 from the National Institutes of Health.

REFERENCES

1. DePianto, D., and P. A. Coulombe. 2004. Intermediate filaments and tissue repair. *Exp. Cell Res.* 301:68–76.
2. Omary, M. B., P. A. Coulombe, and W. H. McLean. 2004. Intermediate filament proteins and their associated diseases. *N. Engl. J. Med.* 351:2087–2100.
3. Coulombe, P. A., M. L. Kerns, and E. Fuchs. 2009. Epidermolysis bullosa simplex: a paradigm for disorders of tissue fragility. *J. Clin. Invest.* 119:1784–1793.
4. Coulombe, P. A., M. E. Hutton, …, E. Fuchs. 1991. Point mutations in human keratin 14 genes of epidermolysis bullosa simplex patients: genetic and functional analyses. *Cell.* 66:1301–1311.
5. Fuchs, E., and D. W. Cleveland. 1998. A structural scaffolding of intermediate filaments in health and disease. *Science.* 279:514–519.
6. Kim, S., and P. A. Coulombe. 2007. Intermediate filament scaffolds fulfill mechanical, organizational, and signaling functions in the cytoplasm. *Genes Dev.* 21:1581–1597.
7. Ma, L., S. Yamada, …, P. A. Coulombe. 2001. A "hot-spot" mutation alters the mechanical properties of keratin filament networks. *Nat. Cell Biol.* 3:503–506.
8. Yamada, S., D. Wirtz, and P. A. Coulombe. 2002. Pairwise assembly determines the intrinsic potential for self-organization and mechanical properties of keratin filaments. *Mol. Biol. Cell.* 13:382–391.
9. Yamada, S., D. Wirtz, and S. C. Kuo. 2000. Mechanics of living cells measured by laser tracking microrheology. *Biophys. J.* 78:1736–1747.

10. Beil, M., A. Micoulet, …, T. Seufferlein. 2003. Sphingosylphosphorylcholine regulates keratin network architecture and visco-elastic properties of human cancer cells. *Nat. Cell Biol.* 5:803–811.

11. Gardel, M. L., J. H. Shin, …, D. A. Weitz. 2004. Elastic behavior of cross-linked and bundled actin networks. *Science.* 304:1301–1305.

12. Storm, C., J. J. Pastore, …, P. A. Janmey. 2005. Nonlinear elasticity in biological gels. *Nature.* 435:191–194.

13. Fuchs, E. 1995. Keratins and the skin. *Annu. Rev. Cell Dev. Biol.* 11:123–153.

14. Sun, T. T., and H. Green. 1978. Keratin filaments of cultured human epidermal cells. Formation of intermolecular disulfide bonds during terminal differentiation. *J. Biol. Chem.* 253:2053–2060.

15. Norlen, L. 2008. Exploring skin structure using cryo-electron microscopy and tomography. *Eur. J. Dermatol.* 18:279–284.

16. Kim, J. S., C.-H. Lee, and P. A. Coulombe. 2010. Modeling the self-organization property of keratin intermediate filaments. *Biophys. J.* 99:2748–2756.

17. Coulombe, P. A., and C.-H. Lee. 2012. Defining keratin protein function in skin epithelia: epidermolysis bullosa simplex and its aftermath. *J. Invest. Dermatol.* 132:763–775.

18. Lulevich, V., H. Y. Yang, …, G. Y. Liu. 2010. Single cell mechanics of keratinocyte cells. *Ultramicroscopy.* 110:1435–1442.

19. Bousquet, O., L. Ma, …, P. A. Coulombe. 2001. The nonhelical tail domain of keratin 14 promotes filament bundling and enhances the mechanical properties of keratin intermediate filaments in vitro. *J. Cell Biol.* 155:747–754.

20. Lee, C.-H., and P. A. Coulombe. 2009. Self-organization of keratin intermediate filaments into cross-linked networks. *J. Cell Biol.* 186: 409–421.

21. Döbereiner, H. G., B. Dubin-Thaler, …, M. P. Sheetz. 2004. Dynamic phase transitions in cell spreading. *Phys. Rev. Lett.* 93:108105.

22. Dubin-Thaler, B. J., J. M. Hofman, …, M. P. Sheetz. 2008. Quantification of cell edge velocities and traction forces reveals distinct motility modules during cell spreading. *PLoS ONE.* 3:e3735.

23. Cuvelier, D., M. Théry, …, L. Mahadevan. 2007. The universal dynamics of cell spreading. *Curr. Biol.* 17:694–699.

24. Xiong, Y., P. Rangamani, …, R. Iyengar. 2010. Mechanisms controlling cell size and shape during isotropic cell spreading. *Biophys. J.* 98: 2136–2146.

25. Dubin-Thaler, B. J., G. Giannone, …, M. P. Sheetz. 2004. Nanometer analysis of cell spreading on matrix-coated surfaces reveals two distinct cell states and STEPs. *Biophys. J.* 86:1794–1806.

26. Wakatsuki, T., R. B. Wysolmerski, and E. L. Elson. 2003. Mechanics of cell spreading: role of myosin II. *J. Cell Sci.* 116:1617–1625.

27. Reinhart-King, C. A., M. Dembo, and D. A. Hammer. 2005. The dynamics and mechanics of endothelial cell spreading. *Biophys. J.* 89:676–689.

28. Yeung, T., P. C. Georges, …, P. A. Janmey. 2005. Effects of substrate stiffness on cell morphology, cytoskeletal structure, and adhesion. *Cell Motil. Cytoskeleton.* 60:24–34.

29. Ponti, A., M. Machacek, …, G. Danuser. 2004. Two distinct actin networks drive the protrusion of migrating cells. *Science.* 305: 1782–1786.

30. Pollard, T. D., and G. G. Borisy. 2003. Cellular motility driven by assembly and disassembly of actin filaments. *Cell.* 112:453–465.

31. Krzyszczyk, P., and C. W. Wolgemuth. 2011. Mechanosensing can result from adhesion molecule dynamics. *Biophys. J.* 101:L53–L55.

32. Potter, D. A., J. S. Tirnauer, …, I. M. Herman. 1998. Calpain regulates actin remodeling during cell spreading. *J. Cell Biol.* 141:647–662.

33. Beningo, K. A., M. Dembo, …, Y. L. Wang. 2001. Nascent focal adhesions are responsible for the generation of strong propulsive forces in migrating fibroblasts. *J. Cell Biol.* 153:881–888.

34. Choi, C. K., M. Vicente-Manzanares, …, A. R. Horwitz. 2008. Actin and α-actinin orchestrate the assembly and maturation of nascent adhesions in a myosin II motor-independent manner. *Nat. Cell Biol.* 10:1039–1050.

35. Dahl, K. N., A. J. Engler, …, D. E. Discher. 2005. Power-law rheology of isolated nuclei with deformation mapping of nuclear substructures. *Biophys. J.* 89:2855–2864.

36. Caille, N., O. Thoumine, …, J. J. Meister. 2002. Contribution of the nucleus to the mechanical properties of endothelial cells. *J. Biomech.* 35:177–187.

37. Laurent, V. M., S. Kasas, …, J. J. Meister. 2005. Gradient of rigidity in the lamellipodia of migrating cells revealed by atomic force microscopy. *Biophys. J.* 89:667–675.

38. Kim, J. S., and S. X. Sun. 2009. Continuum modeling of forces in growing viscoelastic cytoskeletal networks. *J. Theor. Biol.* 256: 596–606.

39. Karcher, H., J. Lammerding, …, M. R. Kaazempur-Mofrad. 2003. A three-dimensional viscoelastic model for cell deformation with experimental verification. *Biophys. J.* 85:3336–3349.

40. Windoffer, R., A. Kölsch, S. Wöll, and R. E. Leube. 2006. Focal adhesions are hotspots for keratin filament precursor formation. *J. Cell Biol.* 173:341–348.

41. Kölsch, A., R. Windoffer, and R. E. Leube. 2009. Actin-dependent dynamics of keratin filament precursors. *Cell Motil. Cytoskeleton.* 66:976–985.

42. Green, K. J., B. Geiger, …, R. D. Goldman. 1987. The relationship between intermediate filaments and microfilaments before and during the formation of desmosomes and adherens-type junctions in mouse epidermal keratinocytes. *J. Cell Biol.* 104:1389–1402.

43. Stamenović, D., and N. Wang. 2000. Invited review: engineering approaches to cytoskeletal mechanics. *J. Appl. Physiol.* 89:2085–2090.

44. Mogilner, A., and G. Oster. 1996. The physics of lamellipodia protrusion. *Eur. Biophys. J.* 25:47–53.

45. Larripa, K., and A. Mogilner. 2006. Transport of a 1D viscoelastic actin-myosin strip of gel as a model of a crawling cell. *Physica A.* 372:113–123.

46. Parsons, J. T., A. R. Horwitz, and M. A. Schwartz. 2010. Cell adhesion: integrating cytoskeletal dynamics and cellular tension. *Nat. Rev. Mol. Cell Biol.* 11:633–643.

47. Bernot, K. M., C.-H. Lee, and P. A. Coulombe. 2005. A small surface hydrophobic stripe in the coiled-coil domain of type I keratins mediates tetramer stability. *J. Cell Biol.* 168:965–974.

48. Dembo, M., and Y. L. Wang. 1999. Stresses at the cell-to-substrate interface during locomotion of fibroblasts. *Biophys. J.* 76:2307–2316.

49. Bottino, D., A. Mogilner, …, G. Oster. 2002. How nematode sperm crawl. *J. Cell Sci.* 115:367–384.

50. Sieg, D. J., C. R. Hauck, and D. D. Schlaepfer. 1999. Required role of focal adhesion kinase (FAK) for integrin-stimulated cell migration. *J. Cell Sci.* 112:2677–2691.

51. Bell, G. I. 1978. Models for the specific adhesion of cells to cells. *Science.* 200:618–627.

52. Weber, G. F., M. A. Bjerke, and D. W. DeSimone. 2012. A mechanoresponsive cadherin-keratin complex directs polarized protrusive behavior and collective cell migration. *Dev. Cell.* 22:104–115.

53. Mendez, M. G., S. Kojima, and R. D. Goldman. 2010. Vimentin induces changes in cell shape, motility, and adhesion during the epithelial to mesenchymal transition. *FASEB J.* 24:1838–1851.

54. Helfand, B. T., M. G. Mendez, …, R. D. Goldman. 2011. Vimentin organization modulates the formation of lamellipodia. *Mol. Biol. Cell.* 22:1274–1289.

55. Karakozova, M., M. Kozak, …, A. Kashina. 2006. Arginylation of β-actin regulates actin cytoskeleton and cell motility. *Science.* 313:192–196.

56. Yoon, K. H., M. Yoon, …, R. D. Goldman. 2001. Insights into the dynamic properties of keratin intermediate filaments in living epithelial cells. *J. Cell Biol.* 153:503–516.

57. Wong, P., and P. A. Coulombe. 2003. Loss of keratin 6 (K6) proteins reveals a function for intermediate filaments during wound repair. *J. Cell Biol.* 163:327–337.

58. Andrä, K., B. Nikolic, …, G. Wiche. 1998. Not just scaffolding: plectin regulates actin dynamics in cultured cells. *Genes Dev.* 12:3442–3451.

59. Foisner, R., F. E. Leichtfried, …, G. Wiche. 1988. Cytoskeleton-associated plectin: in situ localization, in vitro reconstitution, and binding to immobilized intermediate filament proteins. *J. Cell Biol.* 106:723–733.

60. Svitkina, T. M., A. B. Verkhovsky, and G. G. Borisy. 1996. Plectin sidearms mediate interaction of intermediate filaments with microtubules and other components of the cytoskeleton. *J. Cell Biol.* 135:991–1007.

61. Wiche, G. 1998. Role of plectin in cytoskeleton organization and dynamics. *J. Cell Sci.* 111:2477–2486.

62. Osmanagic-Myers, S., M. Gregor, …, G. Wiche. 2006. Plectin-controlled keratin cytoarchitecture affects MAP kinases involved in cellular stress response and migration. *J. Cell Biol.* 174:557–568.

63. Rotty, J. D., and P. A. Coulombe. 2012. A wound-induced keratin inhibits Src activity during keratinocyte migration and tissue repair. *J. Cell Biol.* 197:381–389.

64. Todorović, V., B. V. Desai, …, K. J. Green. 2010. Plakoglobin regulates cell motility through Rho- and fibronectin-dependent Src signaling. *J. Cell Sci.* 123:3576–3586.

65. Barrandon, Y., and H. Green. 1985. Cell size as a determinant of the clone-forming ability of human keratinocytes. *Proc. Natl. Acad. Sci. USA.* 82:5390–5394.

66. Dazard, J. E., J. Piette, …, A. Gandarillas. 2000. Switch from p53 to MDM2 as differentiating human keratinocytes lose their proliferative potential and increase in cellular size. *Oncogene.* 19:3693–3705.

67. Watt, F. M., and H. Green. 1981. Involucrin synthesis is correlated with cell size in human epidermal cultures. *J. Cell Biol.* 90:738–742.

68. Banks-Schlegel, S., and H. Green. 1981. Involucrin synthesis and tissue assembly by keratinocytes in natural and cultured human epithelia. *J. Cell Biol.* 90:732–737.